IEEE Access
Multidisciplinary | Rapid Review | Open Access Journal

Received October 2, 2020, accepted October 11, 2020, date of publication October 21, 2020, date of current version November 3, 2020.

Digital Object Identifier 10.1109/ACCESS.2020.3032929

A Dynamic Artificial Potential Field (D-APF) UAV Path Planning Technique for Following Ground Moving Targets

HERATH MPC JAYAWEERA, (Member, IEEE), AND SAMER HANOUN
Institute for Intelligent System Research and Innovation, Deakin University, Waurn Ponds, VIC 3216, Australia
Corresponding author: Herath MPC Jayaweera (pherathmudiyans@deakin.edu.au)

ABSTRACT Path planning is a vital and challenging component in the support of Unmanned Aerial Vehicles (UAVs) and their deployment in autonomous missions, such as following ground moving target. Few attempts are reported in the literature on multirotor UAV path planning techniques for following ground moving targets despite the great improvement in their control dynamics, flying behaviors and hardware specifications. These attempts suffer several drawbacks including their hardware dependency, high computational requirements, inability to handle obstacles and dynamic environments in addition to their low performance regarding the moving target speed variations. In this paper, a novel dynamic Artificial Potential Field (D-APF) path planning technique is developed for multirotor UAVs for following ground moving targets. The UAV produced path is a smooth and flyable path suitable to dynamic environments with obstacles and can handle different motion profiles for the ground moving target including change in speed and direction. Additionally, the proposed path planning technique effectively supports UAVs following ground moving targets while maneuvering ahead and at a standoff distance from the target. It is hardware-independent where it can be used on most types of multirotor UAVs with an autopilot flight controller and basic sensors for distance measurements. The developed path planning technique is tested and validated against existing general potential field techniques for different simulation scenarios in ROS and gazebo-supported PX4-SITL. Simulation results show that the proposed D-APF is better suited for UAV path planning for following moving ground targets compared to existing general APFs. In addition, it outperforms the general APFs as it is more suitable for UAVs flying in environments with dynamic and unknown obstacles.

INDEX TERMS Unmanned aerial vehicles, path planning, artificial potential field, ground moving targets.

I. INTRODUCTION

A UAV, is a machine capable of flying without a pilot onboard. UAVs have been extensively used by the military for combat purposes [1], reconnaissance [2], and intelligent surveillance [3] during war time. Recently, beyond military purposes, UAVs have been utilized in various civil applications for commercial [4], social [5], and leisure purposes [6].

UAVs are classified as single-rotor, multirotor, fixed-wing, or fixed-wing hybrid, based on their body and propellers configuration. Multirotor UAVs, are those that have more than two propellers and considered the most stable type due to their symmetric structure. Besides, they have distinct advantages compared to other types, such as higher maneuverability and hovering capabilities, robustness, vertical take-off and landing, ability to be easily equipped with different types of sensors, and low maintenance and purchase cost [7]. Therefore, there has been an increasing trend of adopting multirotor UAVs for military and non-military applications [8] such as providing security and conveying protection for mobile targets, capturing live videos and pictures for sport events [9], information collection for better situational awareness [10], and wildlife monitoring [11]. In most scenarios, multirotor UAVs maneuver ahead and at a standoff distance from the target to capture the real-time airborne information required by their mission. In general, for target following missions, adopting tele-operated multirotor UAVs can hinder the mission's effectiveness, while posing a potential impact on humans, due to the required physical and cognitive load to carry the remote controller and remotely pilot the UAV respectively.

The associate editor coordinating the review of this manuscript and approving it for publication was Yangmin Li.

This work is licensed under a Creative Commons Attribution-NonCommercial-NoDerivatives 4.0 License.
For more information, see https://creativecommons.org/licenses/by-nc-nd/4.0/

Therefore, many researchers have been working on an enhanced level of autonomy to increase their efficiency and effectiveness.

Path planning, for multirotor UAVs, is a vital process that can support their deployment ability in autonomous missions such as following a ground moving target (GMT) in dynamic environments with obstacles. In a real world unstructured and dynamic environment, the task of path planning is not limited to following the target movements but also includes determining very quickly a collision-free and smooth flyable path, while fulfilling the mission requirements such as capturing live video information of the target been followed and its surrounding environment. Therefore, the path planning technique needs to be fast and effective in following the GMT when the target rapidly changes its speed and direction. Additionally, the path planner needs to produce adequate dynamics for the multirotor UAV to ensure safe navigation throughout the entire mission. This is because multirotor UAVs are considered dynamically unstable and nonlinear systems [12] as they can easily end up with a catastrophic situation, which could harm humans and the UAV itself, due to minor mistakes in their planned path or generated dynamics.

To date, few attempts have been published in the literature for online path planning techniques for multirotor UAVs to follow a GMT. The majority of existing techniques simplify the path planning problem by considering only two-dimensional path planning in static environments; therefore, they do not fit real world applications as most environments are dynamic, three-dimensional, and unknown [13]. Furthermore, these path planning techniques are not modeled for static and dynamic obstacles avoidance while flying and following a GMT. Finally, most of the existing path planning techniques for following a GMT are developed for fixed-wing UAVs; however, there are other challenges when considering multirotor UAVs. Therefore, an online three-dimensional path planning technique for multirotor UAVs to effectively and quickly follow a GMT in an unknown and dynamic environment is presented in this paper to address the aforementioned gaps and challenges.

The rest of this paper is organized as follows. Section II presents existing literature on moving target following techniques, followed by Section III on the modified general artificial potential fields (APFs). The proposed D-APF technique is described in detail in Section IV. Simulation experiments setup is presented in Section V while the simulation results for different moving target following scenarios using ROS and gazebo-supported PX4-SITL are presented in Section VI, in addition to the performance comparison results against the modified general APFs. Finally, Section VII presents the conclusion of this work.

II. RELATED WORK

Existing techniques for following ground moving targets can be classified into two groups, based on the UAV path planning problem formulation. The first group is concerned with on-time relative localization, including determining the target position information, velocity, and relative distance in a three-dimensional space. For a target, the common known method of localization is cooperative localization, where the target instantly transmits its positional information, acquired from its on-board GPS device, to the UAV, as presented in [14]. Although this method works efficiently and infallibly in open and outdoor environments, it suffers from communication latency and is vulnerable to failure if the direct line of sight between the satellite and the target GPS receiver or the target and the UAV is obstructed by obstacles such as rain clouds and large buildings. The other method is non-cooperative localization, where the UAV onboard sensors are used to sense and identify the target position information relative to the UAV position. As vision sensors are lightweight, low-cost, and information-rich, they are the most commonly used sensors for non-cooperative localization [15] as presented in [16], [17] and [18]. Although non-cooperative vision-based localization shows promising results in indoor and outdoor environments, it fails to determine the position information when a direct line of sight is absent. Also, the target is required to continuously remain in the field of view of the UAV on-board sensors during the entire mission for the UAV to be able to determine its positional information [19]. To avoid the drawbacks of GPS-based localization and vision-based non-cooperative localization, hybrid systems are proposed; [20] and [21] present a localization and tracking system using GPS and visual information where one system can be used if the other system fails. However, using on-board vision sensors for localization increases the system payload and overhead due to the required computational time, in addition to lowering the accuracy of following the target. Since the main focus of this paper is to present a hardware-independent novel path planning technique for following a moving target in an outdoor environment, the GPS-based cooperative localization technique has been adopted to determine the position and velocity components of the moving target.

The second group focuses on navigation and collision avoidance to enable the UAV to follow the target efficiently and safely. Based on the target speed. This group is further subdivided into two classes: 1) target following methods under the constraint of constant speed, and 2) target following methods under the constraint of continuous tracking. Navigation in a circular path [22], circular arcs [23], spiral [24], and sinusoidal [14] paths are the strategies typically used under the constraint of constant speed, where the center of the UAV is moved and synchronized to the target to compensate the difference in speeds. This type of path planning is commonly adopted and more suitable for fixed-wing UAVs due to their limitations of being unable to hover and are required to maintain a minimum airspeed to remain safe in air. These techniques are highly dependent on the use of gimbal cameras for capturing the ambient information of the target specially during obstacle and collision avoidance maneuvers; however, gimbal cameras are expensive to obtain and highly prone to failure.

In contrast, under the constraint of continuous tracking, multirotor UAVs appear more suitable as they have abilities of hovering, making quick turns, and easily changing their velocity. Using proportional-derivative (PD) function [25] and proportional-integral-derivative (PID) function [26] controllers is one of the common techniques for trajectory tracking for following a GMT, but without adequate position and velocity information it would not support both obstacle avoidance and following the target. Introducing a fuzzy logic controller to the PD and PID controllers is another technique used for controlling a UAV to follow a GMT [27], but not without several drawbacks due to their high computational requirements, big overshoot and oscillations (especially with sudden change in the speed and direction of the target), and inability to deal with dynamic obstacles. In [12], a fuzzy-PI based path planning technique for following the movements of mobile vehicles has been presented, along with the simulation and experiment results. Although position updates occur every 22 ms, the path planning process required considerable computational time as the individual 'P' and 'I' gains are calculated based on 49 rules. Moreover, the path planner can only control the UAV roll and pitch, not the yaw angle; therefore, a gimbal camera is necessary and required to capture the target's surrounding as the path planner is unable to control the quadcopter to perform angular movements around its vertical axis, even though it can move omnidirectionally. Inability to detect obstacles and avoid collisions, non-smooth path, and considerable position error are the main drawbacks of this method which they need to be addressed before using it for real-time and in real world applications. Another path planning technique for tracking a GMT with obstacle avoidance for indoor applications using a quadcopter has been proposed in [28], based on the APF method. The UAV is considered as a freely moving mass which is attracted to the target by the attractive force and repelled from obstacles by the repulsive force. The attractive force is a linear function of relative distance and relative velocity between the UAV and target, while the repulsive force is a function of relative distance and velocity between the UAV and obstacle. Although this method has simple computational requirements and is easy to implement, its main drawbacks are the inability to track and follow the target in presence of symmetric obstacles and lack of control to the UAV altitude.

III. GENERAL APF FOR FOLLOWING MOVING TARGETS

Based on their simplicity and ease of use, APF methods are often used for path planning and navigation of UAVs. The concept behind the APF method is to construct a virtual attractive field for the target position and virtual repulsive fields for the obstacles. The attractive field pulls the UAV towards the target, while the repulsive fields push away the UAV from the obstacles, so the UAV moves towards the target while avoiding collisions with the obstacles under the resultant force. When following a GMT, the potential function cannot be expressed only as a function of relative distance but must also incorporate the target's relative velocity [28], [29]. In general, there are two types of potential functions: the general APF (G-APF) and general exponential APF (GE-APF).

A. GENERAL APF (G-APF) FUNCTION

The G-APF function presented in [28] is a quadratic function of relative position and relative velocity; hence, it is a linear function of relative distance and relative velocity, where the force increases unlimitedly with the relative velocity and relative distance. To suit a multirotor UAV with a maximum acceleration and velocity, this paper proposes a modification to the G-APF attractive potential function (U_a) by including two sub potential functions, an attractive potential function due to the relative position ($U_a(q)$) and an attractive potential function due to the relative velocity ($U_a(v)$). Both sub potential functions handle the X and Y spatial dimensions. The modified G-APF attractive potential function and its sub potential functions are given as follows;

$$U_a(q) = \begin{cases} \frac{k_1}{2}(q_t - q_m)^2; & q_{t,m} \le q_d \\ k_3(q_t - q_m); & q_{t,m} > q_d, \end{cases} \tag{1}$$

$$U_a(v) = \begin{cases} \frac{k_2}{2}(v_t - v_m)^2; & v_{t,m} \le v_d \\ k_4(v_t - v_m); & v_{t,m} > v_d, \end{cases} \tag{2}$$

$$U_a = U_a(q) + U_a(v), \tag{3}$$

$q_t = [x_t, y_t]^T$ and $q_m = [x_m, y_m]^T$ are the position coordinates of the target and UAV respectively. The velocities of the target and UAV are represented using v_t and v_m respectively, while $q_{t,m}$ and $v_{t,m}$ are the relative position and relative velocity respectively of the target with respect to the UAV. q_d and v_d are the parabolic range of displacement and velocity respectively. k_1 to k_4 are positive scale factors.

Similarly, this paper proposes a modification to the G-APF repulsive potential function (U_r) by including two sub potential functions, a repulsive potential function due to the relative distance ($U_r(q)$) and a repulsive potential function due to the relative velocity ($U_r(v)$). The modified G-APF repulsive potential function and its sub potential functions are given as follows;

$$U_r(q) = \begin{cases} 0; & q_{o,m} > q_c \\ \dfrac{-r_1}{2(q_{o,m} - q_e)^2}; & q_{o,m} \le q_c, \end{cases} \tag{4}$$

$$U_r(v) = \begin{cases} 0; & v_{o,m} \ge 0 \\ \dfrac{-r_2}{2}(v_o - v_m)^2; & v_{o,m} < 0, \end{cases} \tag{5}$$

$$U_r = U_r(q) + U_r(v), \tag{6}$$

r_1 and r_2 are positive scale factors and $q_{o,m}$ is the distance between the nearest obstacle and the UAV, considered as the difference between the obstacle's position q_o and the UAV's position q_m. v_o is the velocity of the obstacle. q_c and q_e represent the distance sensor range and minimum distance between the UAV and the obstacle respectively.

Both the attractive and repulsive forces (F_a) and (F_r) can be derived from the negative gradients of their corresponding potential functions. These are expressed as follows;

$$F_a = -\frac{\partial U_a(q)}{\partial q} - \frac{\partial U_a(v)}{\partial v}, \tag{7}$$

$$F_a = \begin{cases} k_1 q_{t,m} + k_2 v_{t,m}; & q_{t,m} \le q_d, v_{t,m} \le v_d \\ \dfrac{q_{t,m}}{|q_{t,m}|} k_3 + k_2 v_{t,m}; & q_{t,m} > q_d, v_{t,m} \le v_d \\ k_1 q_{t,m} + \dfrac{v_{t,m}}{|v_{t,m}|} k_4; & q_{t,m} \le q_d, v_{t,m} > v_d \\ \dfrac{q_{t,m}}{|q_{t,m}|} k_3 + \dfrac{v_{t,m}}{|v_{t,m}|} k_4; & q_{t,m} > q_d, v_{t,m} > v_d, \end{cases} \tag{8}$$

$$F_r = -\frac{\partial U_r(q)}{\partial q} - \frac{\partial U_r(v)}{\partial v}, \tag{9}$$

$$F_r = \begin{cases} 0; & q_{o,m} \ge q_c \\ \dfrac{-r_1\, q_{o,m}}{|(q_{o,m} - q_e)^3\, q_{o,m}|}; & q_{o,m} \le q_c, v_{o,m} \ge 0 \\ \dfrac{-r_1\, q_{o,m}}{|(q_{o,m} - q_e)^3\, q_{o,m}|} & \\ -r_2 v_{o,m}; & q_{o,m} \le q_c, v_{o,m} < 0. \end{cases} \tag{10}$$

The attractive force consists of four different components based on the limitations of relative distance and relative velocity between the target and the UAV. The force is a linear function of relative distance and relative velocity until it reaches the threshold level, and then it switches to a constant value, as the force generated should be equal to or below the maximum force that can be achieved by the multirotor UAV. The attractive force will reach zero if and only if $v_{t,m}$ and $q_{t,m}$ reach zero.

B. GENERAL EXPONENTIAL APF (GE-APF) FUNCTION

The general exponential APF function is commonly used for path planning of unmanned ground vehicles and unmanned sea vehicles; however, it can be adopted for UAV path planning. In a similar fashion, to modifying the G-APF, the modified attractive and repulsive forces can be defined as follows;

$$F_a = \frac{q_{t,m}}{|q_{t,m}|}\left[k_{a1}(1 - e^{-b_1 q_{t,m}^2}) + k_{a2}(1 - e^{-b_2 v_{t,m}^2})\right], \tag{11}$$

$$F_r = -\frac{q_{o,m}}{|q_{o,m}|}\left[k_{r1}\, e^{-b_3 q_{o,m}^2} + k_{r2}(1 - e^{-b_4 v_{o,m}^2})\right]; v_{o,m} < 0, \tag{12}$$

k_{a1} and k_{a2} are the gain factors of the attractive force, where their summation produces the maximum attractive force. The gain factors of the repulsive force are denoted as k_{r1} and k_{r2}, where their summation gives the maximum repulsive force. b_1, b_2, b_3, and b_4 are positive constants that contribute to identifying the required minimum velocity and minimum displacement that generate the maximum attractive and repulsive forces.

IV. DYNAMIC APF (D-APF) PATH PLANNING FOR FOLLOWING MOVING TARGETS

The proposed dynamic potential field-based path planning technique is inspired by the moving target following methods presented in [12] and [28]. However, to overcome their hardware dependency drawback, the proposed technique is formulated to provide the waypoints required by the UAV on-board autopilot; therefore, relying on the UAV PID controller to handle its dynamics and flying behavior. A novel attractive and repulsive forces are proposed to handle dynamic environments and obstacles avoidance, in addition, to reacting to the change of speed and direction of the moving target. The proposed D-APF requires two types of inputs; the GMT position information and UAV position from its onboard sensors where the GMT position information are used to calculate the velocity information and heading field. Using these two inputs, the D-APF path planner generates the attractive force for following the GMT while creating the repulsive force to navigate a collision free path.

A. D-APF ATTRACTIVE FORCE

To follow the movements of a target with variable velocity, the attractive force needs to change rapidly when the UAV is near to the target; however, the attractive force, magnitude should smoothly increase with the relative distance until it reaches its maximum. To achieve these requirements, the proposed D-APF adopts an exponential attractive function since a linear potential function has a fixed gradient for its force to relative displacement while an exponential potential function has a varying gradient for its force. The proposed D-APF adopts an exponential attractive function that consists of three sub forces for its attractive force: a force due to the relative distance in the XY plane ($F_a(q)$), a force due to the relative velocity in the XY plane ($F_a(v)$) and a force due to the relative distance in the vertical plane ($F_a(z)$), where the total attractive force is acquired by the vector summation of the three individual sub forces. These are expressed as follows;

$$F_a(q) = \frac{q_{t,m}}{|q_{t,m}|} k_{p1}(1 - e^{-c_1 |q_{t,m} - e_0|}), \tag{13}$$

$$F_a(v) = \frac{v_{t,m}}{|v_{t,m}|} k_{p2}(1 - e^{-c_2 |v_{t,m}|}), \tag{14}$$

$$F_a(z) = \frac{(q_{zt} - q_{zm})}{|q_{zt} - q_{zm}|} k_{p3}(1 - e^{-c_3 |h + q_{zt} - q_{zm}|}), \tag{15}$$

$$F_a = F_a(q) + F_a(v) + F_a(z), \tag{16}$$

k_{p1}, k_{p2} and k_{p3} are the gain factors of the attractive force, where the maximum attractive force in the horizontal plane is given by the summation of $k_{p1} + k_{p2}$. The maximum attractive force in the vertical direction is given by k_{p3}. c_1, c_2 and c_3 are positive constants where c_1 and c_3 are used for controlling the minimum relative displacement required to achieve the maximum force. e_0 is the standoff distance where $e_0 > 0$ and $e_0 < 0$ represent scenarios where the GMT is followed by negative and positive standoff distances respectively. c_2 is used for controlling the minimum relative velocity required

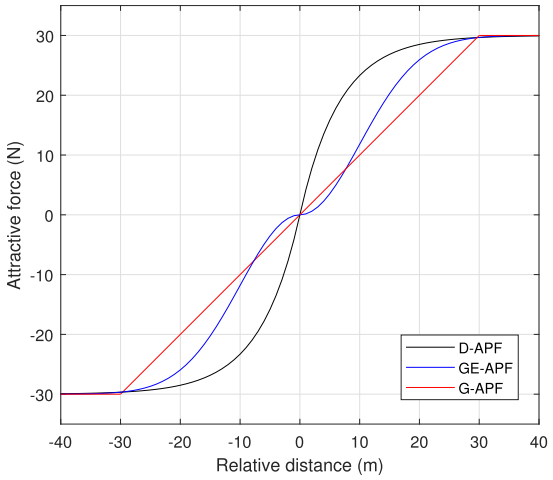

FIGURE 1. Variation in the attractive force with the relative distance.

for achieving the maximum force. q_{zm} and q_{zt} represent the Z coordinates of the UAV and the target respectively, where h is the pre-defined relative distance in the vertical axis.

The variation in the attractive force with the relative distance for the proposed D-APF and general modified APFs are depicted in Fig. 1, where the gradient near to zero relative distance is higher for the proposed D-APF compared to the general APFs. This higher gradient can create a higher magnitude of attractive force for a small change of relative distance. It can help the UAV to quickly and effectively follow the movement of the GMT when the GMT varies its velocity. Further, the proposed D-APF has a better smooth variation of attractive force compared to the general APFs. A similar shape of variation can be observed for the relative velocity when $q_{t,m} = 0$. Considering the above factors, the attractive force of the proposed D-APF is more suitable for UAV path planning for following moving targets.

B. D-APF REPULSIVE FORCE

Trees and bridges are few examples of typical obstacles faced by UAVs while following a GMT; however, these are not the same obstacles for the ground moving target. Existing GMT following techniques including general APFs, generate the UAV collision avoidance path only in the XY plane. They suffer from different drawbacks such as local minima, inability to find a path when facing symmetric obstacles and ineffectively following the GMT when obstacles are nearby. To overcome these drawbacks, the proposed D-APF adopts an exponential repulsive function that considers obstacle avoidance and plans the UAV collision free path in the 3D space. This is achieved by ensuring that the proposed repulsive force is active mainly in the vertical direction where a collision free path is generated for the UAV by changing its vertical position when obstacles are in its path as shown in Fig. 2. Therefore, an additional horizontal directional repulsive force is proposed to prevent any collision in case the vertical force is not capable of avoiding the obstacle.

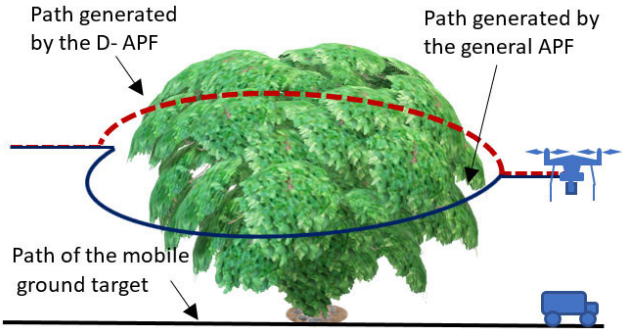

FIGURE 2. UAV planned paths by the D-APF and general APFs for obstacle avoidance.

The proposed repulsive force of the D-APF is a function of the relative distance and relative velocity between the obstacle and the UAV as it consists of forces in the horizontal direction due to the relative distance ($F_r(q)$) and relative velocity ($F_r(v)$). These are defined as follows;

$$F_r(q) = -\frac{q_{o,m}}{|q_{o,m}|} k_{n1}\, e^{-c_3|q_{0,m}|}, \tag{17}$$

$$F_r(v) = -\frac{v_{o,m}}{|v_{o,m}|} k_{n2}(1 - e^{-c_4|v_{0,m}|});\ v_{0,m} < 0. \tag{18}$$

The gain factors of the repulsive force are denoted as k_{n1} and k_{n2} where the maximum repulsive force is given by the summation of $k_{n1} + k_{n2}$. c_3 and c_4 are positive constants and contribute to controlling the minimum relative distance and relative velocity required to achieve a zero repulsive force.

Fig. 3, depicts the variation in the horizontal direction repulsive force generated by the proposed D-APF and general APFs for the obstacle relative distance. Both, the proposed D-APF and GE-APF have the advantage of gradient change; however, the gradient change of the GE-APF decreases only near to the origin, but the proposed D-APF gradient is better and generates higher repulsive force. In addition, the proposed D-APF repulsive force has simpler mathematical formulation compared to the repulsive force of the G-APF. According to (17), larger c_3 can generate rapid changes in the repulsive force; smaller c_3 generates smoother and slower changes in the repulsive force with the relative distance. A large c_3 value such as $c_3 > 5$ can be used to ensure that the main objective of this repulsive force in the XY plane is to avoid any sudden collisions that are unable to be handled by the change in the vertical position.

The forces in the vertical axis due to obstacles and the resultant force are defined as follows;

$$F_r(z1) = k_{p4}\, e^{-c_5|q_{0,m}\cos\theta|};\ \begin{cases} |q_{0,m}|\sin\theta < h_0 \\ and \\ |q_{0,m}| < h_0 \end{cases}, \tag{19}$$

$$F_r(z2) = k_{p5}\, e^{-c_6|v_{0,m}|};\ \begin{cases} v_{0,m} < 0 \\ and \\ |q_{0,m}| < h_2, \end{cases} \tag{20}$$

$$F_r = F_r(q) + F_r(v) + F_r(z1) + F_r(z2), \tag{21}$$

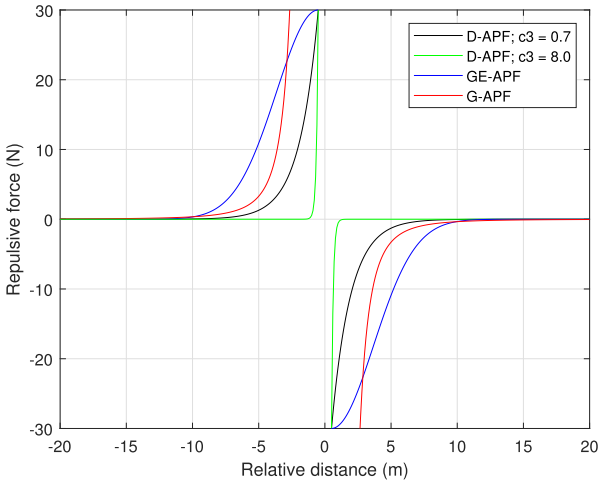

FIGURE 3. Variation of repulsive forces with obstacle relative distance.

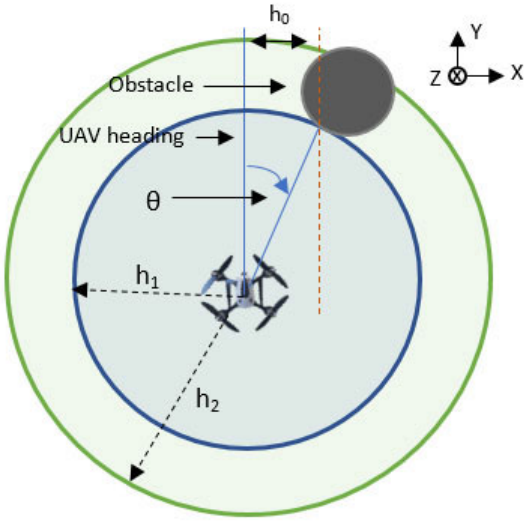

FIGURE 4. Representation of parameters in (19) and (20).

k_{p4} and k_{p5} are the gain factors that control the maximum force generated from (19) and (20) respectively. The positive constants c_5 and c_6 are less than 1.0; therefore, the UAV will receive the vertical directional force before the repulsive force in the XY plane. This will ensure that the vertical position changes when obstacles are nearby to avoid any collisions, but in worst case scenario, if the change in the vertical position is insufficient, the repulsive force in the XY plane is activated for collision avoidance. $2h_0$ is the width of the GMT, while θ represents the angle between the obstacle and the UAV heading as shown in Fig. 4. The GMT width is assumed to be greater than the UAV width.

C. WAYPOINT GENERATION

Velocity and position waypoints are the typical inputs of any UAV using an autopilot such as the Ardupilot [30] and PX4 [31]; however, using velocity waypoints has an advantage over position waypoints in controlling both the UAV speed and trajectory. The analytical expression of the velocity waypoint ($v_{t+\Delta t}$) is presented in (22), where v_t and m represent the GMT velocity and mass of the UAV respectively. The data transfer frequency from the path planner to the autopilot is represented by $f (f = 1/\Delta t)$.

$$v_{t+\Delta t} = \left(\frac{1+f}{f}\right) v_t + \frac{(F_a + F_r)}{mf}. \tag{22}$$

The position information of the GMT used in the velocity calculations is defined as follows;

$$v_t = nf(q_t - q_{t-n\Delta t}), \tag{23}$$

n is a positive number and $q_{t-n\Delta t}$ is the position data of the GMT before $n\Delta t$.

V. SIMULATION SETUP

The proposed D-APF path planning technique has been implemented using the robot operating system (ROS) [32]. To evaluate its performances and compare it against the general modified APFs, realistic simulation scenarios have been created in Gazebo supported with the PX4 Software in the Loop (SITL) simulation. Details of the simulation experiments setup are presented in the following sections.

A. GMT, UAV AND ENVIRONMENT MODELS

PX4 SITL has a mobile vehicle called "r1-rover" that is available for unmanned ground vehicle simulation. This vehicle, shown in Fig. 5, has been adopted to simulate the GMT. It has a maximum velocity of 1 m/s (i.e., 3.6 km/h) and its motion can only be controlled via velocity waypoints which makes it unable to follow appropriately a desired path due to the lack of position waypoints. To overcome these limitations, the vehicle maximum velocity is modified to 8 m/s (i.e., 28.8 km/h), velocity waypoints yaw angle is utilized to enable the vehicle to perform turns around its Z-axis without changing its X and Y coordinates and its differential drive steering is supported with position waypoints to enable it better control in following a desired path with minimum deviation.

The PX4 SITL "irish" UAV, shown in Fig. 5, has been used to simulate the multirotor UAV. The UAV model has an Inertial Measurement Unit (IMU) for determining its speed and heading, Global Positioning System (GPS) for position information, Micro Air Vehicle Link (MAVLink) receiver for receiving positional data from the ground vehicle, and two distance measurement sensors for obstacle detection purposes. These two sensors are located at the front and the base of the UAV for forward and downward obstacle detection. The PX4 autopilot supported by the PX4 flight controller has been utilized for controlling the dynamics of the UAV. The velocity and yaw angle fields of the UAV autopilot waypoints have been employed for the UAV to follow the GMT according to the GMT speed and to control the UAV heading subject to the GMT received direction.

Different simulation environments that resemble real world scenarios have been created in Gazebo. These environments, shown in Fig. 6 (a) to (c), are generally wide open plain

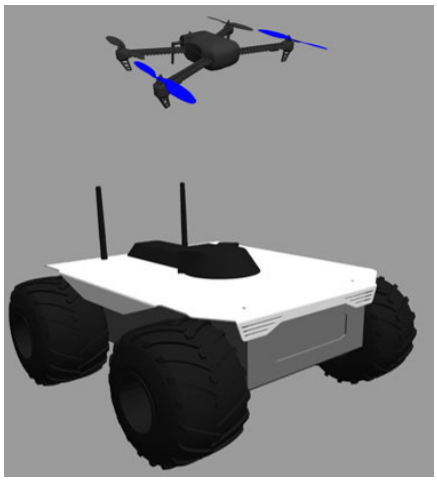

FIGURE 5. PX4 SITL "r1-rover" and "irish" adopted to simulate the GMT and multirotor UAV.

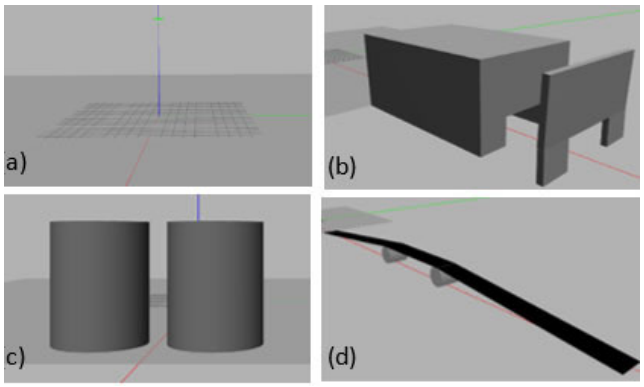

FIGURE 6. Simulation environments a- obstacle-free, b- with two bridges of height 15 m, c- with two cylinders situated 2 m apart, d- dynamic obstacle-free tilted path.

terrain environments where some are free of obstacles while others have obstacles such as bridges with a height of 15 m and cylinders with radius of 5 m, height of 15 m and are situated 2 m apart on the opposite sides of the GMT path. The environment shown in Fig. 6 (d) is an obstacle-free dynamic environment that has a tilted path with an altitude increments of 1 m for a 10 m of horizontal displacement. These environments support the GMT to travel for several kilometers, if needed; however, for the sake of results presentation, the GMT traveled distance is limited to 1 km in both X and Y directions.

B. GMT MOTION PROFILES

Two velocity profiles for the GMT motion have been considered in the simulation experiments: a constant velocity motion profile and a variable velocity motion profile. To simulate these profiles, the position, velocity and yaw angle waypoints fields have been used for producing the GMT motion. The constant velocity motion profile employed a 1000 m (1 km) straight-line path, 4000 m (4 km) square path and 242 m circular path, as shown in Fig. 7, for evaluating the

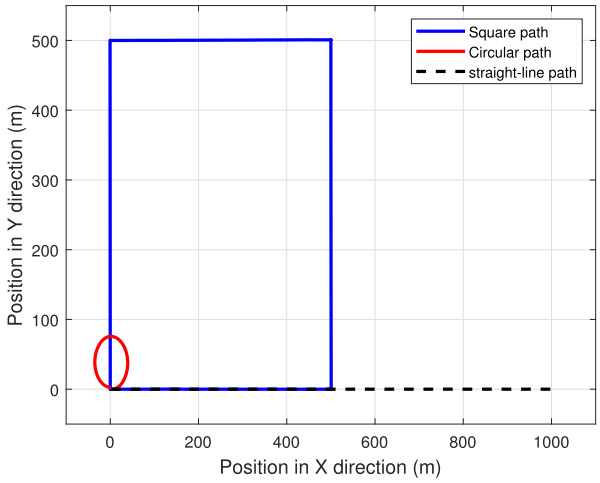

FIGURE 7. GMT straight-line, square and circular paths.

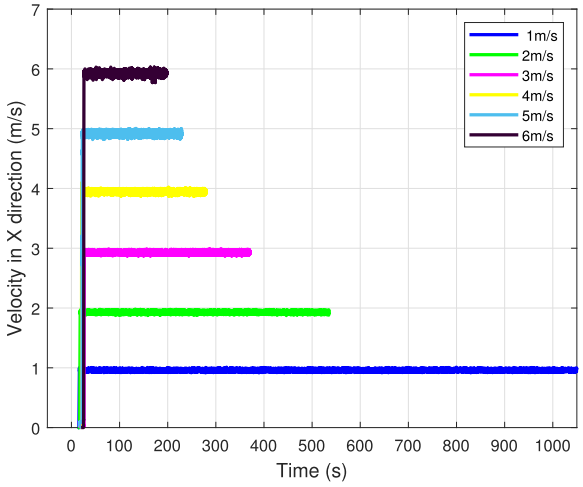

FIGURE 8. GMT adopted constant velocities.

performance of the proposed D-APF in following the GMT. The initial position coordinates of the GMT are set at (1, 0, 0) for different constant velocities 1 m/s to 6 m/s as shown by the velocities graph in Fig. 8.

The variable velocity motion profile used velocity waypoints to vary the velocity of the GMT for the desired range of position waypoints along a 1000 m (1 km) straight-line path. Fig. 9, shows the GMT variable velocity along with its corresponding position graph in Fig. 10.

VI. SIMULATION RESULTS

A. D-APF PERFORMANCE EVALUATION

To validate the behavior of the proposed D-APF path planning technique and the UAV generated path for following the GMT, six simulation experiments have been conducted with the GMT moving in different shaped paths with constant and variable velocities.

The first experiment validates the D-APF performance when the GMT is moving in a 1000 m straight-line path along the X-direction with a constant velocity of 4 m/s.

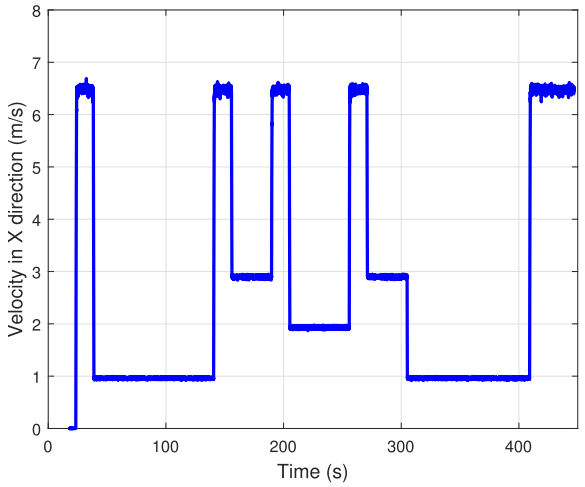

FIGURE 9. GMT variable velocity motion profile.

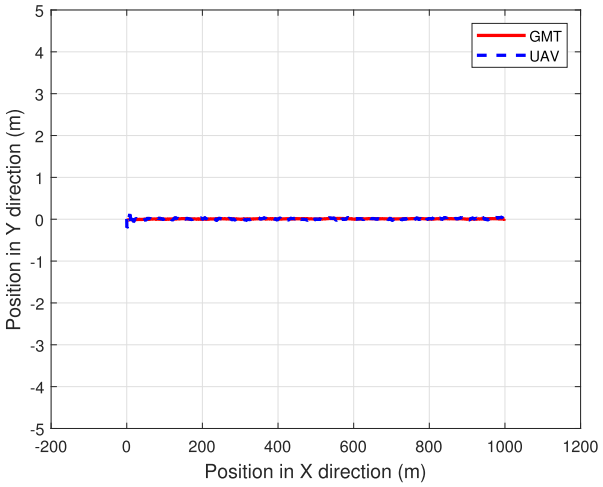

FIGURE 12. UAV path in 2D for the GMT straight-line path.

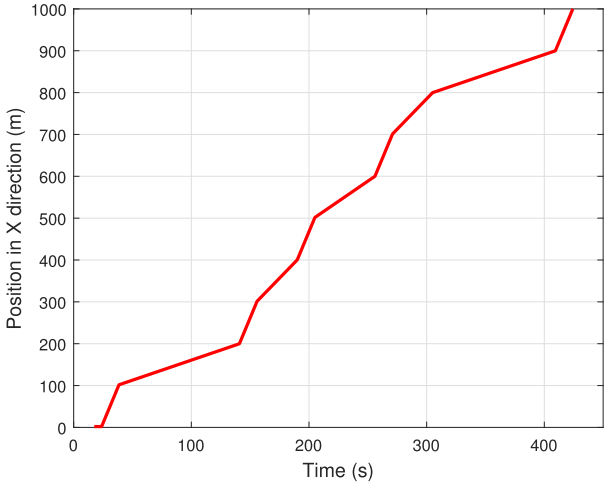

FIGURE 10. GMT position for the variable velocity motion profile.

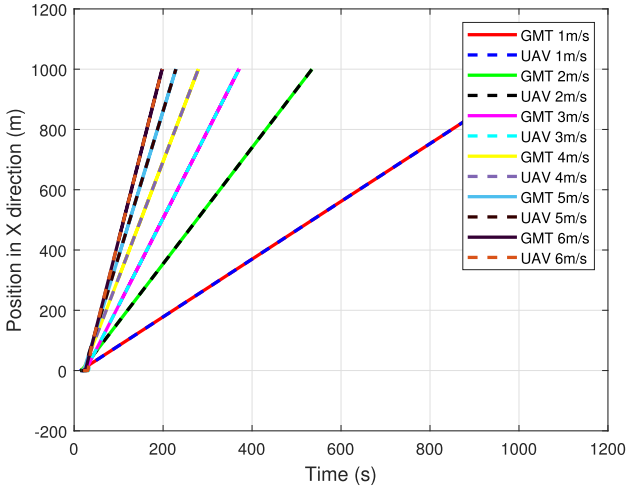

FIGURE 13. UAV position in X-direction vs time for the GMT different constant velocities.

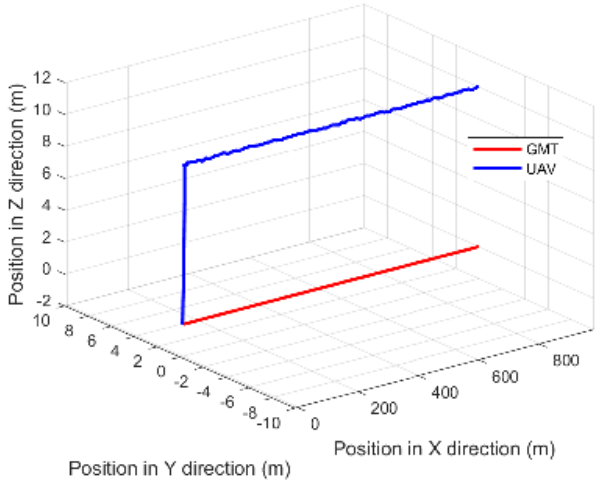

FIGURE 11. UAV planned path in 3D for the GMT straight-line path.

Fig. 11 shows the GMT and UAV simulated 3D paths. The GMT and UAV initial positions are $(1, 0, 0)$ and $(0, 0, 0)$ respectively and both start their motions simultaneously where the GMT moves horizontally, and the UAV moves vertically. The UAV starts its horizontal motion once it reaches an altitude of 10 m. It can be observed from Fig. 12, that the paths for both the GMT and the UAV are smooth and straight. The resultant relative position of the UAV in the X-direction with respect to the GMT has a mean value of 0.0155 m and standard deviation of 0.0967 m.

The second experiment examines the D-APF performance when the GMT is moving in a 1000 m straight-line path along the X-direction with constant velocities from 1 m/s to 6 m/s. Fig. 13 shows the position versus time graph for the GMT and UAV. The GMT and UAV initial positions are $(1, 0, 0)$ and $(0, 0, 0)$ respectively and both start their motions simultaneously where the GMT moves horizontally, and the UAV moves vertically. The UAV starts its horizontal motion once it reaches an altitude of 10 m. Although the UAV position is coincident with the GMT position as shown in Fig. 13; the average relative displacement of the UAV in the X-direction with respect to the GMT has a maximum mean value of 0.082 m and standard deviation of 0.185 m

TABLE 1. Simulation results of the D-APF for the GMT different constant velocities for a 1000 m path.

GMTV (m/s)	MO (m)	ARD in X (m)	SD of RD in X (m)	ARD in Y (m)	SD of RD in Y (m)	ARD in Z (m)	SD of RD in Z (m)	UAVV from Fig. 13 (m/s)	UAVV from Fig. 14 (m/s)
1	0.30	0.0065	0.0241	0.0007	0.0116	10.001	0.0074	0.998	0.998
2	0.43	-0.0255	0.0422	0.0008	0.0139	10.001	0.0078	2.001	2.001
3	0.57	-0.0080	0.0799	0.0004	0.0143	10.002	0.0107	3.001	3.001
4	0.70	0.0155	0.0967	-0.0006	0.0186	10.001	0.0096	3.999	3.999
5	0.82	0.0572	0.1598	-0.0033	0.0276	10.006	0.0201	4.996	4.996
6	0.96	0.0815	0.1843	-0.0061	0.0310	10.004	0.0187	5.989	5.989

GMTV - GMT velocity, MO – maximum overshoot, ARD in X – average relative displacement in X-direction, SD of RD in X – standard deviation of relative displacement in X-direction, ARD in Y – average relative displacement in Y-direction, SD of RD in Y – standard deviation of relative displacement in Y-direction, ARD in Z – average relative displacement in Z-direction, SD of RD in Z – standard deviation of relative displacement in Z-direction, UAVV – UAV velocity.

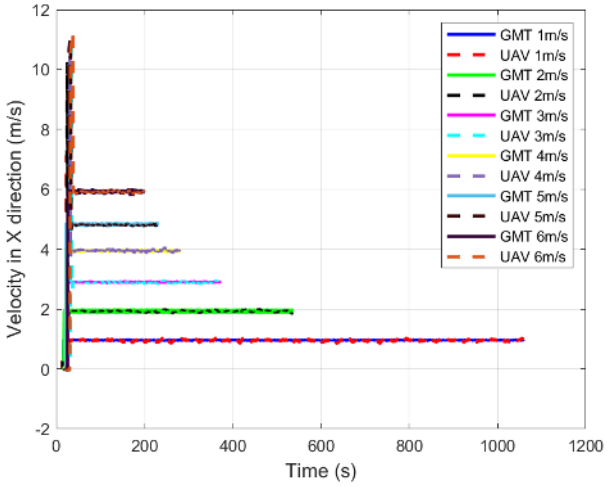

FIGURE 14. UAV velocity in X-direction vs time for GMT constant velocities.

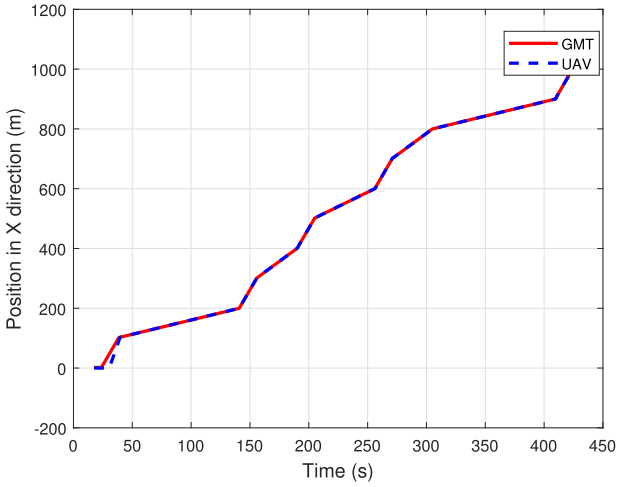

FIGURE 15. UAV position in X-direction vs time for GMT variable velocity.

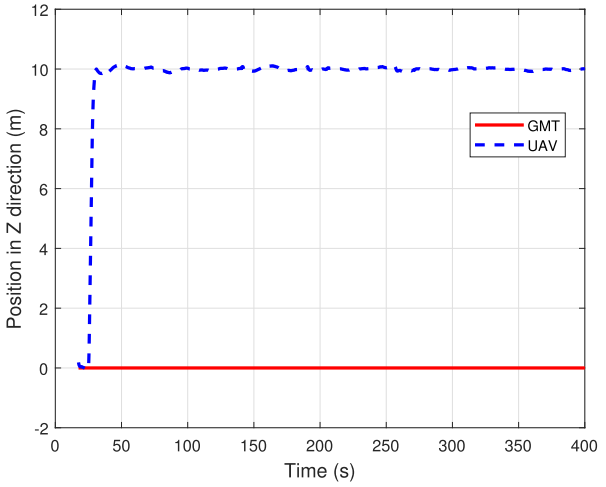

FIGURE 16. UAV position in Z-direction vs time for the GMT straight-line path.

as depicted in Table. 1. The average relative displacement in the Y-direction has a maximum mean value of 0.0061 m and standard deviation of 0.0310 m at GMT velocity of 6 m/s where the standard deviation increases with the GMT velocity. Fig. 14 shows the velocity versus time graph for the GMT and UAV. It can be observed that the gradient of Fig. 13 is equal to the corresponding UAV velocity given in Fig. 14 as depicted in Table 1. In addition, the UAV velocity approaches the GMT velocity once it is positioned above it, as confirmed in Table 1; then the UAV follows the GMT accurately.

The third experiment tests the D-APF performance when the GMT is moving in a 1000 m straight-line along the X-direction with a variable velocity between 1 m/s to 6.5 m/s that changes as shown in Fig. 9. The GMT and UAV initial positions are (1, 0, 0) and (0, 0, 0) respectively and both start their motion simultaneously where the GMT moves horizontally, and the UAV moves vertically. The UAV starts its horizontal motion once it reaches an altitude of 10 m. Fig. 15 shows the position versus time graph for the GMT and UAV where the UAV position coincides with the GMT position except during the initial 15 s. The UAV has -2.1 m overshoot at 141.3 s for the velocity variation from 1 m/s to 6.5 m/s, 1.2 m overshoot at 156.4 s for the velocity variation from 6.5 m/s to 3 m/s, -0.9 m overshoot at 190.5 s for the velocity variation from 3 m/s to 6.5 m/s, 1.5 m overshoot

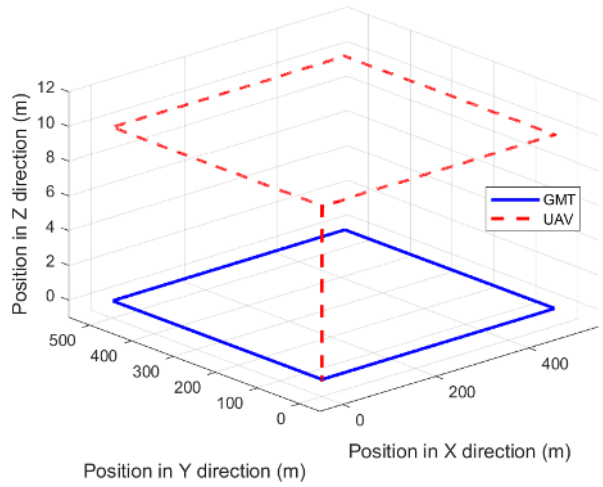

FIGURE 17. UAV path in 3D for the GMT square path.

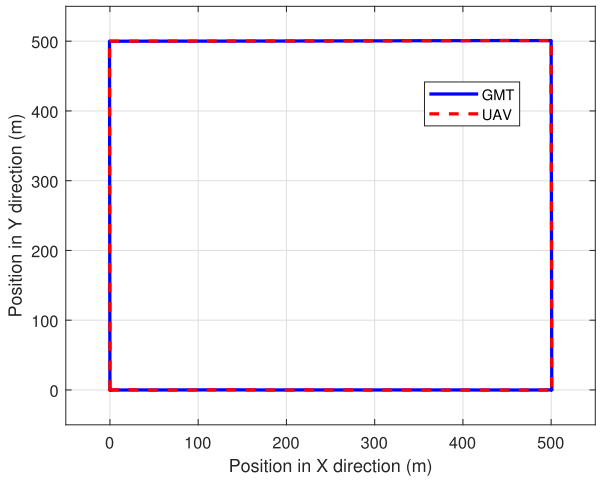

FIGURE 18. UAV path in 2D for the GMT square path.

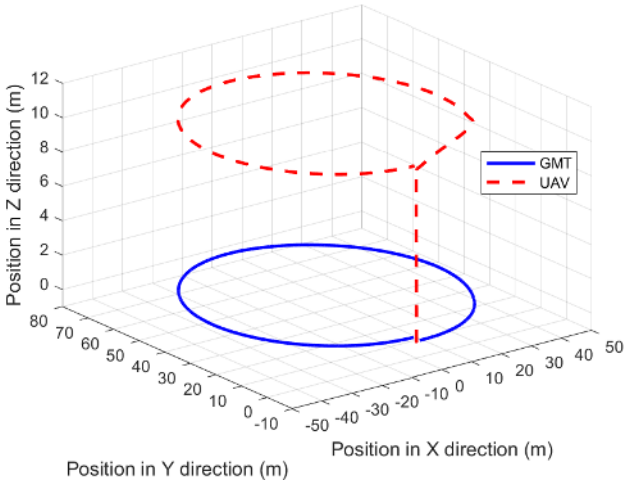

FIGURE 19. UAV path in 3D for the GMT circular path.

at 205.7 s for the velocity variation from 6.5 m/s to 2 m/s, 0.6 m overshoot at 305.6 s for the velocity variation from 2 m/s to 6.5 m/s, and -2 m overshoot at 402.1 s for the velocity variation from 3 m/s to 1 m/s. The D-APF shows its capability

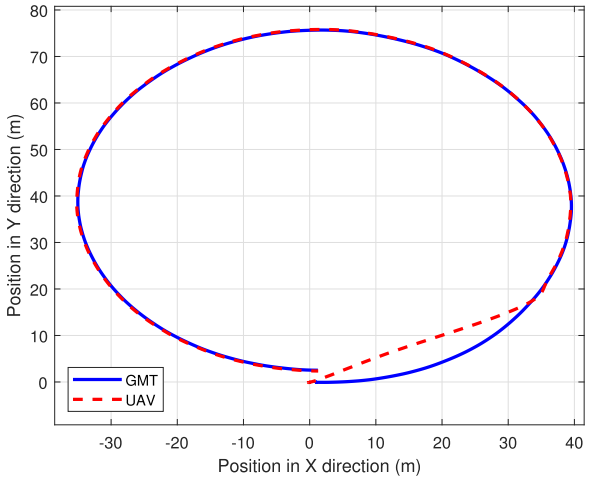

FIGURE 20. UAV path in 2D for the GMT circular path.

of handling this overshoot within less than 2 s as then the UAV follows the GMT accurately without any overshoots. It can be observed from Fig. 16 that the UAV maintains accurately its altitude during the time where the GMT varies its velocity. The resultant relative position of the UAV in the Z-direction with respect to the GMT has a mean value of 9.998 m and standard deviation of 0.038 m.

In addition to the straight-line motion of the GMT, the proposed D-APF can successfully control the UAV to follow the GMT while moving on different shaped paths. The fourth experiment evaluates the D-APF performance when the GMT is moving in a 4000 m square path with a constant velocity of 4 m/s. The GMT and UAV initial positions are $(1, 0, 0)$ and $(0, 0, 0)$ respectively and both start their motion simultaneously where the GMT moves horizontally, and the UAV moves vertically. The UAV starts its horizontal motion once it reaches an altitude of 10 m. Fig. 17 and Fig. 18 show the respective 3D and 2D paths of the UAV when the GMT is moving in the square path. The UAV has 2% average position error and 1.4 m overshoot at each corner of the square path in the horizontal direction. The resultant relative position of the UAV in the Z-direction with respect to the GMT has a mean value of 9.9955 m and standard deviation of 0.0116 m.

The fifth experiment assesses the D-APF performance when the GMT is moving in a 242 m circular path in an anticlockwise direction with a constant speed of 4 m/s. The GMT and UAV initial positions are $(1, 0, 0)$ and $(0, 0, 0)$ respectively and both start their motion simultaneously where the GMT moves horizontally, and the UAV moves vertically. The UAV starts its horizontal motion once it reaches an altitude of 10 m. Fig. 19 and Fig. 20 shows the respective 3D and 2D paths of the GMT and UAV when GMT is moving in the circular path. It can be seen that the UAV path and GMT paths are equal except for the first 13.6 s; first the UAV takes-off vertically until it reaches an altitude of 10 m, moves in a straight-line to catch-up with the GMT before it starts following it in the circular path. This simulation

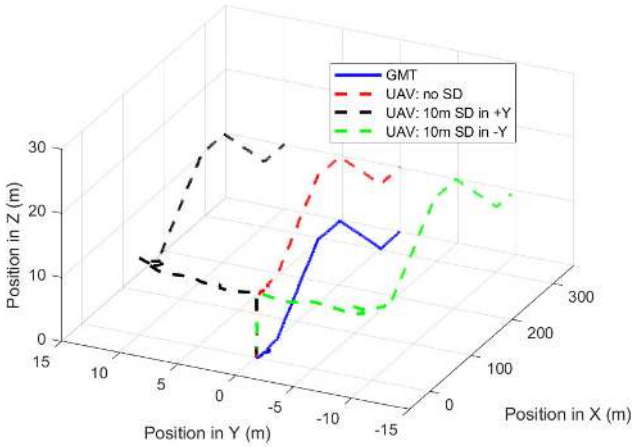

FIGURE 21. UAV 3D position following the GMT with and without standoff distances.

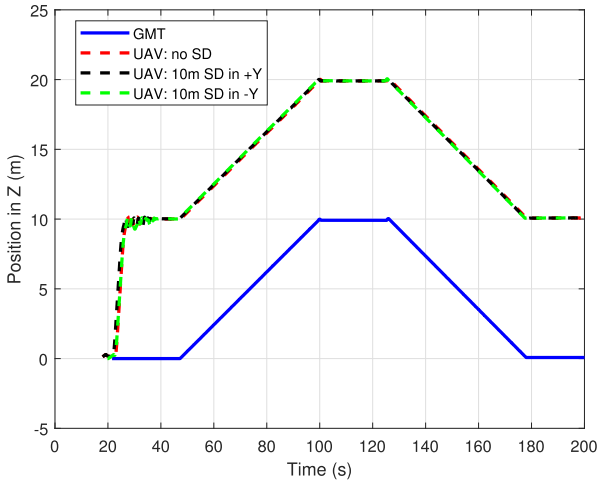

FIGURE 22. UAV altitude for the GMT elevated path.

experiment shows that the proposed D-APF is sensitive for a small change of relative displacement and that the UAV can successfully follow the movement of the GMT while maintaining its position above the GMT regardless of its speed and direction.

The sixth experiment illustrates the capability of the D-APF for following the GMT with a standoff distance when the GMT is moving in an elevated dynamic path along the X-direction with a constant velocity of 2 m/s. The GMT and UAV initial positions are (1, 0, 0) and (0, 0, 0) respectively and both start their motion simultaneously where the GMT moves horizontally, and the UAV moves vertically. The UAV starts its horizontal motion once it reaches a relative altitude of 10 m. Fig. 21 shows the 3D positions of the GMT and the UAV with and without standoff distances during the GMT motion in the elevated dynamic path. The corresponding altitude variation is depicted in Fig. 22 where the UAV synchronizes its altitude with the GMT and continues at 10 m relative altitude distance along the Z-axis as set during the simulation experiment, regardless of its current standoff distance. The resultant relative position of the UAV in the Z-direction with respect to the GMT has a mean value of 10.002 m and standard deviation of 0.012 m with and without standoff distances. The resultant relative position of the UAV in the X-direction with respect to the GMT has a mean value of -0.0256 m and standard deviation of 0.0424 m. This experiment shows that the D-APF is better suited for the following the GMT with and without standoff distances.

B. D-APF PERFORMANCE COMPARISON TO GENERAL APFs

To compare the performance of the proposed D-APF against the general modified APFs, four experiments have been conducted with the GMT moving along the positive X-direction with different velocities, then gradually stops and changes heading by turning around its Z-axis to the opposite direction before moving back along the negative X-direction to its initial position. These experiments examine the UAV generated path for the D-APF against the general modified APFs in terms of displacement, overshoot and settlement time subject to the GMT speed and change in direction. In each experiment, the GMT and UAV initial positions are (1, 0, 0) and (0, 0, 0) respectively and both start their horizontal motion simultaneously. During the initial few seconds, before the GMT starts its motion, the UAV change its yaw angle to align its heading with the GMT heading in the positive X-direction.

In the first experiment, the GMT velocity has been set at 0.5 m/s, to provide the ability of evaluating the proposed D-APF against the general APFs for following targets moving with very slow speeds. The GMT starts its motion at 15 s and moves 5 m in the positive X-direction, then rotates around its Z-axis to the opposite direction in heading during the time interval from 25 s to 44 s, before initiating a backward motion to its initial position. Fig. 23 shows the comparison of the D-APF to the general APFs in terms of UAV and GMT displacements. Although, both the proposed D-APF and general APFs have close results, in terms of their displacements, the proposed D-APF exhibited better performance. The GE-APF, G-APF and D-APF have 0.9 m, 0.08 m and 0.04 m average relative displacement (position error) respectively along the X-direction; which shows that the D-APF has the lowest position error compared to the general APFs. The D-APF has smaller oscillations regarding the GMT change of velocity which illustrates its higher stability. The GE-APF, G-APF and D-APF have 0.50 m, 0.22 m and 0.15 m maximum overshoot respectively along the X-direction; which indicates that the D-APF has the lowest overshoot compared to the general APFs. Besides the D-APF has 0.15 s maximum settlement time which is the minimum compared to the general APFs. Therefore, according to the position error, overshoot and settlement time, the D-APF is better suited for following very slow moving targets with velocity around 0.5 m/s; this is because the attractive force of the D-APF rapidly adapts to small changes of relative displacement and relative velocity even when the relative displacement and relative velocity are close to zero.

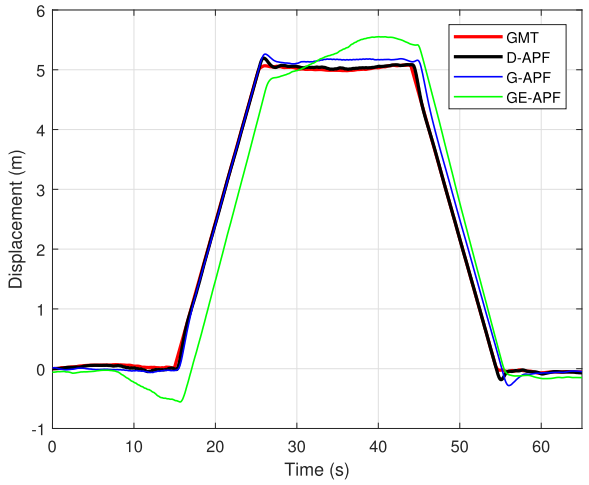

FIGURE 23. Comparison of D-APF and general APFs in terms of displacement for the GMT velocity of 0.5 m/s.

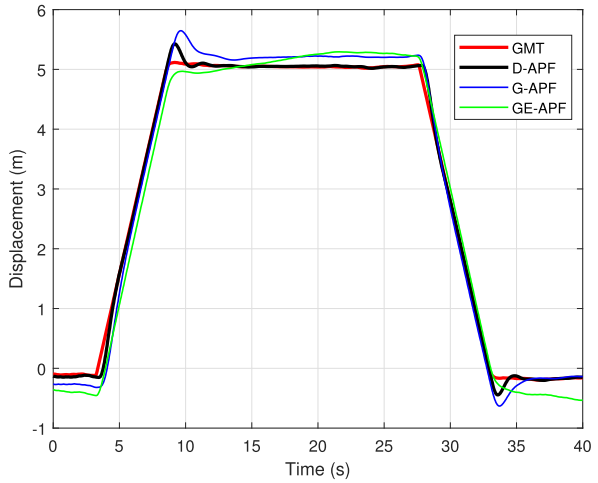

FIGURE 24. Comparison of D-APF and general APFs in terms of displacement for the GMT velocity of 1.0 m/s.

In the second experiment, the GMT velocity has been set at 1 m/s, to provide the ability of evaluating the proposed D-APF for following targets moving with slow speeds. The GMT starts its motion at 3 s and moves 5 m in the positive X-direction, then rotates around its Z-axis to the opposite direction in heading during the time interval from 8.7 s to 28.7 s, before initiating a backward motion to its initial position. Fig. 24 shows the comparison of the D-APF to the general APFs in terms of UAV and GMT displacements. The GE-APF, G-APF and D-APF have 0.373 m, 0.098 m and 0.068 m average relative displacement (position error) respectively along the X-direction; which shows that the D-APF has the lowest position error compared to the general APFs. Although, the GE-APF has the lowest overshoot, the largest settlement time of the GE-APF shows that it has lower sensitivity for a small change of relative displacement. The D-APF has 0.302 m overshoot at 9.08 s and the G-APF has 0.507 m overshoot at 9.60 s during velocity change from 1 m/s to 0 m/s. Furthermore, the D-APF has smaller oscillations regarding the GMT change of velocity which illustrates its higher stability. Therefore, according to the position error, overshoot and settlement time, the D-APF is better suited for following slow moving targets with velocity around 1 m/s; this is because the attractive force of D-APF rapidly adapts to small changes in relative displacement and relative velocity even when the relative displacement and relative velocity are close to zero.

In the third experiment, the GMT velocity has been set at 3 m/s, to provide the ability of evaluating the proposed D-APF for following targets moving with slow to average speeds. The GMT start its motion at 8.5 s and moves 20 m in the positive X-direction, then rotates around its Z-axis to the opposite direction in heading during the time interval from 15.3 s to 33.9 s, before initiating a backward motion to its initial position. Fig. 25 shows the comparison of the D-APF to the general APFs in terms of UAV and GMT displacements. The GE-APF, G-APF and D-APF have 0.096 m, 0.053 m and 0.008 m average relative displacement (position error) respectively along the X-direction; which shows that the D-APF has the lowest position error compared to the general APFs. It can be clearly seen that the GE-APF has the lowest oscillations and overshoots compared to the G-APF and D-APF; however, the D-APF has the lowest settlement time which is less than 2 s. Moreover, the GE-APF and D-APF have 0.9 m and 0.04 m of average relative displacement respectively during the time interval from 15.3 s to 33.9 s. Therefore, according to the position error, overshoot and settlement time, the D-APF is better suited for following slow to average moving targets with velocity around 3 m/s; this is because the attractive force of D-APF rapidly adapts to small changes in relative displacement and relative velocity even when the relative displacement and relative velocity are close to zero.

In the fourth experiment, the GMT velocity has been set at 5 m/s, to provide the ability of evaluating the proposed D-APF for following targets moving with average speeds. The GMT starts its motion at 5.5 s and moves 20 m in positive X-direction, then rotates around its Z-axis to the opposite direction in heading during the time interval from 10.3 s to 29.3 s before initiating a backward motion to its initial position. Fig. 26 shows the comparison of the D-APF to the general APFs in terms of UAV and GMT displacement. The GE-APF, G-APF and D-APF have 0.166 m, 0.101 m and 0.054 m average relative displacement (position error) and 0.82 m, 2.51 m and 1.01 m overshoot respectively along the X-direction; however, the D-APF path is closer to the GMT path and has lower oscillations. Additionally, the D-APF settlement time is 2.4 s which is the lowest compared to the general APFs. Therefore, according to the position error, overshoot and settlement time, the D-APF is better suited for the GMT following average moving with velocity around 5 m/s; this is because the attractive force of D-APF rapidly adapts to small changes in relative displacement and relative velocity even when the relative displacement and relative velocity are close to the zero.

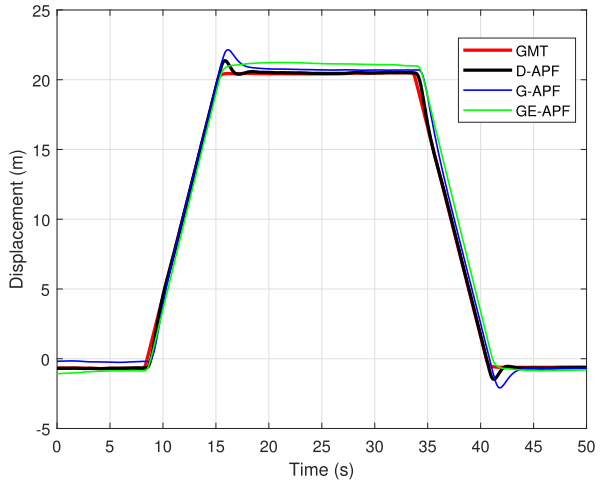

FIGURE 25. Comparison of D-APF and general APFs in terms of displacement for the GMT velocity of 3.0 m/s.

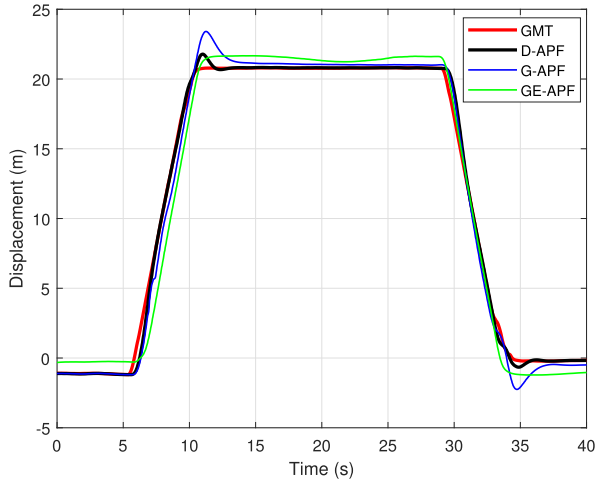

FIGURE 26. Comparison of D-APF and general APFs in terms of displacement for the GMT velocity of 5.0 m/s.

C. D-APF PERFORMANCE FOR OBSTACLE AVOIDANCE

To evaluate the performance of the D-APF and its obstacle avoidance ability, three simulation experiments have been conducted for the GMT moving in a straight-line along the X-direction at a constant velocity of 3 m/s. The GMT and UAV initial positions are $(1, 0, 0)$ and $(0, 0, 0)$ respectively and both start their motion simultaneously where the GMT moves horizontally, and the UAV moves vertically for 6.3 s to reach an altitude of 10 m before it starts following the GMT in the horizontal direction.

In the first experiment, a horizontal cylinder with a radius of 5 m and length of 20 m has been placed at $(60, 0, 10)$, to provide the ability of evaluating the proposed D-APF for obstacle avoidance when a curve-shaped object is in the path of the UAV. The horizontal cylinder has been placed on top of the two cubic-shaped obstacles with a height of 5 m to create a surface with a total height of 15 m, where the cylinder is considered only as an obstacle in the UAV path but not at the GMT path. Fig. 27 shows the GMT and UAV simulated 3D paths. It can be clearly seen that the UAV can avoid the obstacle by varying its altitude while following the GMT when the curved surface or object is in its path. The UAV has 0.087 m average relative displacement and 0.103 m standard deviation respectively along the X-direction. This is because the repulsive force is perpendicular to the attractive force and the attractive force mainly controls the horizontal motion as the repulsive force affects only the vertical motion. Therefore, the obstacle has minimum impact on the UAV path while following the GMT in the horizontal direction.

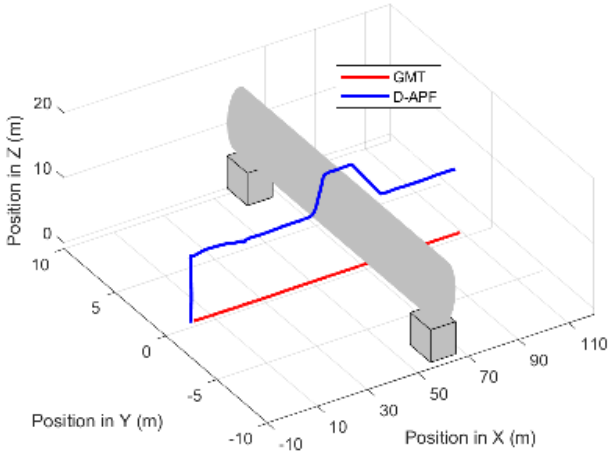

FIGURE 27. UAV planned path avoiding a curved obstacle such as a bridge.

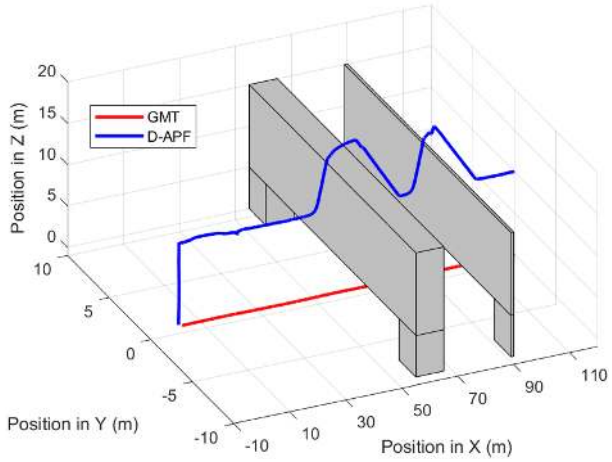

FIGURE 28. UAV planned path avoiding two flat obstacles 30 m apart in the forward direction.

In the second experiment, two flat obstacles with width of 10 m and height of 15 m, width of 1 m and height of 15 m have been placed at 60 m and 90 m in the X-direction from the origin, to provide the ability of evaluating the proposed D-APF for obstacle avoidance when the vertical flat-shaped objects are in the path of the UAV. This bridge shaped objects are obstacles only in the UAV path but not in the GMT path. Fig. 28 shows the GMT and UAV simulated 3D paths. The UAV has 0.091 m average relative displacement and 0.132 m standard deviation respectively along the X-direction.

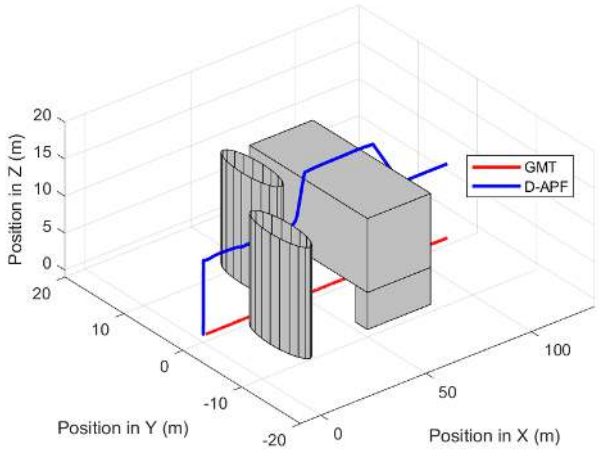

FIGURE 29. UAV planned path avoiding complex obstacles.

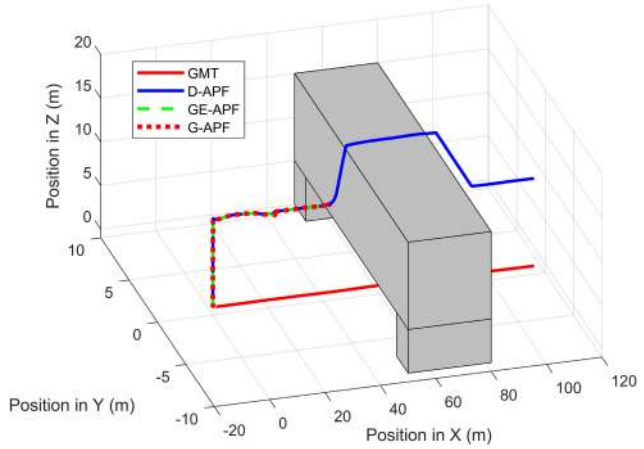

FIGURE 30. UAV planned path by the D-APF and general APFs following the GMT and avoiding a flat obstacle such as a bridge of 15 m height, 30 m width and 20 m length.

In the third experiment, two cylinders with a radius of 5 m and height of 15 m and a flat obstacle with a width of 30 m and height of 15 m have been placed at (30, −6, 0), (40, 6, 0) and (70, 0, 0) respectively, to provide the ability of evaluating the proposed D-APF for obstacle avoidance when the vertical flat objects are in the path of the UAV. Fig. 29 shows the GMT and UAV simulated 3D paths. The UAV has 0.087 m average relative displacement and 0.126 m standard deviation respectively along the X-direction. It can be seen that the repulsive force has no effect on the UAV path if the obstacles are apart with a distance of more than 1.0 m. These results show the capability of the proposed D-APF in generating a valid and efficient path for following the GMT while avoiding obstacles with different types and shapes.

D. D-APF PERFROMANCE COMPARISON TO GENERAL APFs FOR OBSTACLE AVOIDANCE

To compare the performance of the proposed D-APF against the general APFs for obstacle avoidance, two simulation experiments have been conducted for the GMT moving in a straight-line along the X-direction with a constant velocity of 3 m/s. The GMT and UAV initial positions are (1, 0, 0) and (0, 0, 0) respectively and both start their motion simultaneously where the GMT moves horizontally, and the UAV moves vertically for 6.3 s to reach an altitude of 10 m before it starts following the GMT in the horizontal direction.

In the first experiment, the GMT passes under a flat object such as a bridge with a height of 15 m, width of 30 m and length of 20 m that is placed at (70, 0, 0). Fig. 30 shows the 3D plot of the GMT and UAV generated paths by the D-APF and general APFs. The general APFs fail to generate the UAV required path to continuously follow the GMT when this obstacle is in the UAV path; the UAV oscillates in the X-direction where the amplitude of the oscillations increases with time and then decreases until they reach zero. on the contrary, the D-APF continuously follows the GMT and avoids the obstacle by changing the UAV altitude until the obstacle is avoided. The UAV then goes back to its desired altitude of 10 m to continue following the GMT.

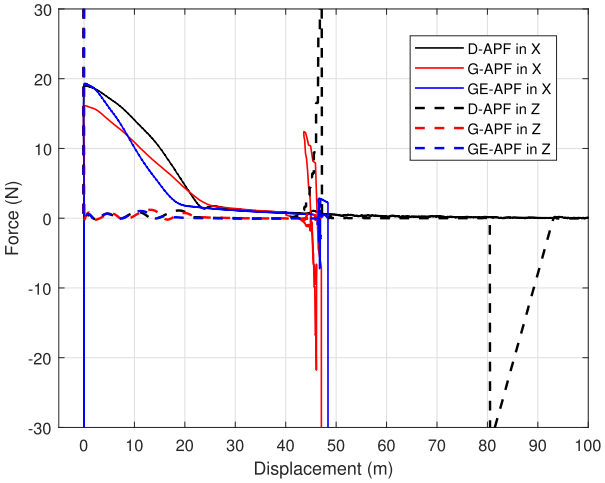

FIGURE 31. The resultant force vs displacement for the D-APF and general APFs while following the GMT and avoiding a flat obstacle such as a bridge of 15 m height, 30 m width and 20 m length.

Fig. 31 shows the resultant force versus displacement for the D-APF and general APFs. The resultant force in the X-direction has its maximum positive value at zero displacement due to the large relative displacement between the UAV and GMT, then it decreases with the displacement as the UAV approaches closer to the obstacle. The resultant force on the UAV due to the general APFs starts to increase when the UAV passes the point (45, 0, 10). This force is opposite to the direction of motion; therefore, the UAV moves in the X-direction. This leads to increase in the attractive force due to the increase of the relative distance between the UAV and GMT, while the repulsive force decreases due to the increase of the relative distance between the UAV and the obstacle. As a result of the resultant force, the UAV moves towards the obstacle with a higher velocity and approaches the obstacle very closely based on the high generated repulsive force. This process continues until the attractive force reaches its maximum due to the relative displacement between the UAV

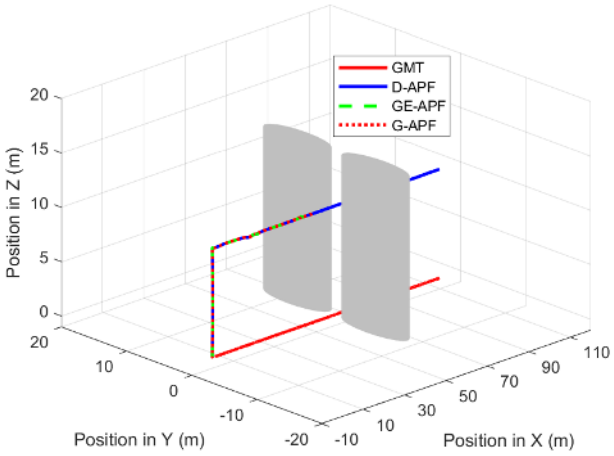

FIGURE 32. UAV planned path by the D-APF and general APFs following the GMT and avoiding two obstacles (cylinders) that are 2 m apart.

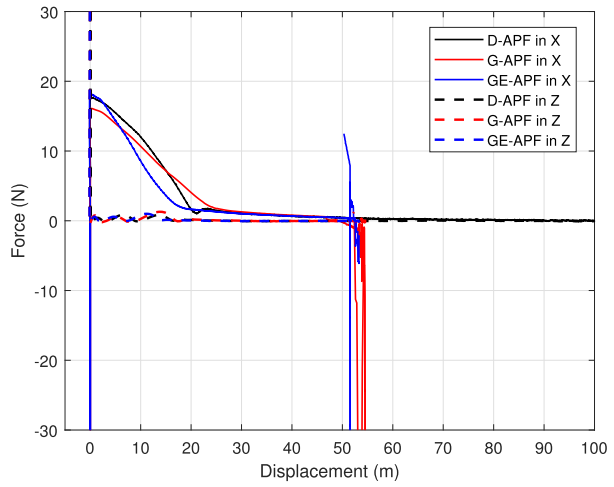

FIGURE 33. The resultant force vs displacement for the D-APF and general APFs while following the GMT and avoiding two obstacles (cylinders) that are 2 m apart.

and GMT. The resultant force of the D-APF in the X-direction has no change nearby the obstacle; therefore, the UAV continuously follow the movement of the GMT in the horizontal direction. The resultant force of the D-APF in the Z-direction has sudden positive and negative peaks when the UAV is in displacement of 46 m and 81 m respectively. This is due to that the minimum distance to the obstacle is at 46 m where the vertical force is maximum while at 81 m the repulsive force will reach zero; therefore, the attractive force in the Z-axis is maximum as the UAV has higher relative displacement (relative displacement between the desired altitude and UAV altitude) in the Z-axis.

In the second experiment, the GMT passes between two symmetrical cylinders with a radius of 5 m and height of 15 m, positioned at (60, -6, 0) and (60, 6, 0) and spaced apart by 2 m. This experiment is used to compare the performance of the D-APF against general APFs for symmetrical obstacles with narrow passages such as trees and buildings. Fig. 32 shows the 3D plot of the GMT path and UAV generated paths by the D-APF and general APFs. It can be seen that only the proposed D-APF can successfully follow the GMT, avoiding the obstacles while moving safely through the narrow passage. Again, the general APFs fail due to their horizontal repulsive force; however, the proposed D-APF can handle such scenario. Fig. 33 shows the resultant force versus displacement for the D-APF and general APFs. The resultant force of the D-APFs and general APFs in the Z-direction and X-direction have similar variations during the initial displacement of 45 m, then only the D-APF has unchanged resultant force. This is because, the D-APF repulsive force is only affected when the obstacles are closer than 0.8 m in sideways to the UAV path. The horizontal repulsive force of the general APFs generates oscillations around the displacement of 45 m due to the increase of repulsive and attractive forces.

VII. CONCLUSION

This paper presented the design of a novel dynamic APF-based (D-APF) online three-dimensional path planning technique for multirotor UAVs to effectively follow ground moving targets in unknown and dynamic environments. The proposed D-APF path planning technique is hardware-independent, can handle various types and shapes of 3D obstacles and has better performance regarding changes in the GMT velocity and direction. D-APF allows precise following of the GMT with constant and variable velocities based on an attractive force that changes rapidly when the UAV is near to the target with its magnitude smoothly increasing with the relative distance until reaching its maximum. Moreover, the D-APF repulsive force plans the UAV collision free path in the 3D space as being active mainly in the vertical direction; however, supported with a horizontal component to prevent any collision in case the vertical force is not capable of avoiding the obstacle. Compared to the general APFs, the D-APF attractive force has a better smooth variation with high gradient near to zero relative distance to help the UAV to quickly and effectively follow the movement of the GMT when the GMT varies its velocity while its repulsive force has a simpler mathematical formulation, smooth variation and slower change with the relative distance with higher gradient in the XY plane to avoid sudden collisions that might occur due to the change in the UAV vertical position.

The performance of the proposed D-APF path planning technique has been validated in various realistic simulation scenarios where the GMT moves in various shaped paths (i.e., straight-line, square and circular) with different constant and variable velocities. The D-APF has shown an average position error (relative displacement) of 0.65%, 0.8% and 8.15% per meter in the moving target direction of motion, position error standard deviation of 0.0241 m, 0.0799 m and 0.1843 m and overshoot of 0.30 m, 0.57 m and 0.96 m for the GMT velocities of 1 m/s, 3 m/s and 6 m/s respectively. Further, the D-APF has a capability of handling the overshoot within less than 2s when the GMT varies its velocity, while maintaining accurate altitude during that time. This is in

addition to maintaining a 2% average position error and 1.4 m overshoot at each corner when following the GMT while moving in a square path along the horizontal direction. Not to mention, the D-APF ability to follow the GMT with and without standoff distances while keeping its relative altitude distance along the Z-axis with the GMT when moving on an elevated dynamic path along the X-direction.

The proposed D-APF has been compared against the general APFs in scenarios where the GMT moves with various velocities, 0.5 m/s, 1 m/s, 3 m/s and 5 m/s and changes its heading by turning to the opposite direction around its Z-axis. The D-APF has shown superiority to the general APFs in terms of lowest position error, smaller oscillations regarding the GMT change of velocity which illustrates its higher stability, lowest overshoot and minimum settlement time. This is mainly due to its attractive force being able to rapidly adapt to small changes of the GMT relative displacement and relative velocity even when they are close to zero. In light of obstacle avoidance, the D-APF showed great capability in planning the UAV path avoiding simple and complex 3D obstacles such as curved cylinders and flat cubes while the general APFs failed causing the UAV to oscillate in the X-direction as the amplitude of the oscillations increased with time then decreased until reaching zero. The D-APF ability to handle these obstacles is due to the no change in its resultant force in the X-direction nearby the obstacles which enables the UAV to continuously follow the movement of GMT in the horizontal direction. This also helps the UAV to move safely through narrow passages between obstacles as the D-APF repulsive force is only affected when the obstacles are closer than 0.8 m in sideways to the UAV path.

Future work will consider enhancing the proposed D-APF to handle other types and shapes of obstacles and basically to avoid losing the line of sight of the GMT while avoiding obstacles as this is crucial in real world applications and a fundamental objective for a UAV following ground moving targets.

REFERENCES

[1] V. Boulanin and M. Verbruggen, "Availability and military use of UAVs," Dept. Dutch Ministry Foreign Affairs, SIPRI Literature Rev. Policy Oper. Eval., Tech. Rep., Aug. 2017, pp. 121–132.

[2] J. Y. C. Chen, "UAV-guided navigation for ground robot tele-operation in a military reconnaissance environment," *Ergonomics*, vol. 53, no. 8, pp. 940–950, Aug. 2010.

[3] J. T. Butler, "UAVs and ISR sensor technology," Air Command Staff College, Maxwell Air Force Base, Montgomery, AL, USA, Tech. Rep. AU/ACSC/033/2001-04, 2001.

[4] M. C. Tatum and J. Liu, "Unmanned aircraft system applications in construction," *Procedia Eng.*, vol. 196, pp. 167–175, Jan. 2017.

[5] L. Merino, F. Caballero, J. R. Martínez-de Dios, J. Ferruz, and A. Ollero, "A cooperative perception system for multiple UAVs: Application to automatic detection of forest fires," *J. Field Robot.*, vol. 23, nos. 3–4, pp. 165–184, 2006.

[6] I. Mademlis, V. Mygdalis, N. Nikolaidis, M. Montagnuolo, F. Negro, A. Messina, and I. Pitas, "High-level multiple-UAV cinematography tools for covering outdoor events," *IEEE Trans. Broadcast.*, vol. 65, no. 3, pp. 627–635, Sep. 2019.

[7] Y. Li and C. Liu, "Applications of multirotor drone technologies in construction management," *Int. J. Construct. Manage.*, vol. 19, no. 5, pp. 401–412, Sep. 2019.

[8] J. Irizarry and D. B. Costa, "Exploratory study of potential applications of unmanned aerial systems for construction management tasks," *J. Manage. Eng.*, vol. 32, no. 3, May 2016, Art. no. 05016001.

[9] V. Iastrebov, C. Y. Wong, W. C. Pang, and G. Seet, "Motion tracking drone for extreme sports filming," 2014.

[10] R. Geraldes, A. Goncalves, T. Lai, M. Villerabel, W. Deng, A. Salta, K. Nakayama, Y. Matsuo, and H. Prendinger, "UAV-based situational awareness system using deep learning," *IEEE Access*, vol. 7, pp. 122583–122594, 2019.

[11] S. Radiansyah, M. Kusrini, and L. Prasetyo, "Quadcopter applications for wildlife monitoring," *IOP Conf. Ser. Earth Environ. Sci.*, vol. 54, no. 1, 2017, Art. no. 012066.

[12] M. Rabah, A. Rohan, S. A. Mohamed, and S.-H. Kim, "Autonomous moving target-tracking for a UAV quadcopter based on fuzzy-pi," *IEEE Access*, vol. 7, pp. 38407–38419, 2019.

[13] P. Yao, H. Wang, and Z. Su, "Real-time path planning of unmanned aerial vehicle for target tracking and obstacle avoidance in complex dynamic environment," *Aerosp. Sci. Technol.*, vol. 47, pp. 269–279, Dec. 2015.

[14] J. Lee, R. Huang, A. Vaughn, X. Xiao, J. K. Hedrick, M. Zennaro, and R. Sengupta, "Strategies of path-planning for a UAV to track a ground vehicle," in *Proc. AINS Conf.*, 2003, pp. 1–6.

[15] X. Wang, H. Zhu, D. Zhang, D. Zhou, and X. Wang, "Vision-based detection and tracking of a mobile ground target using a fixed-wing UAV," *Int. J. Adv. Robotic Syst.*, vol. 11, no. 9, p. 156, Sep. 2014.

[16] Y. Watanabe and P. Fabiani, "Optimal guidance design for UAV visual target tracking in an urban environment," *IFAC Proc. Volumes*, vol. 43, no. 15, pp. 69–74, 2010.

[17] R. P. George and V. Prakash, "Real-time human detection and tracking using quadcopter," in *Intelligent Embedded Systems*. Singapore: Springer, 2018, pp. 301–312.

[18] D. B. Barber, J. D. Redding, T. W. McLain, R. W. Beard, and C. N. Taylor, "Vision-based target geo-location using a fixed-wing miniature air vehicle," *J. Intell. Robotic Syst.*, vol. 47, no. 4, pp. 361–382, Nov. 2006.

[19] J.-M. Li, C. W. Chen, and T.-H. Cheng, "Estimation and tracking of a moving target by unmanned aerial vehicles," in *Proc. Amer. Control Conf. (ACC)*, Jul. 2019, pp. 3944–3949.

[20] H. Huang, L. Zhang, C. Fu, Y. Zhou, and Y. Tian, "Ground moving target tracking algorithm for multi-rotor unmanned aerial vehicle," in *Proc. Chin. Control Decis. Conf. (CCDC)*, Jun. 2018, pp. 1214–1219.

[21] P. Chen, Y. Dang, R. Liang, W. Zhu, and X. He, "Real-time object tracking on a drone with multi-inertial sensing data," *IEEE Trans. Intell. Transp. Syst.*, vol. 19, no. 1, pp. 131–139, Jan. 2018.

[22] T. H. Summers, M. R. Akella, and M. J. Mears, "Coordinated standoff tracking of moving targets: Control laws and information architectures," *J. Guid., Control, Dyn.*, vol. 32, no. 1, pp. 56–69, Jan. 2009.

[23] X. Chu Ding, A. R. Rahmani, and M. Egerstedt, "Multi-UAV convoy protection: An optimal approach to path planning and coordination," *IEEE Trans. Robot.*, vol. 26, no. 2, pp. 256–268, Apr. 2010.

[24] M. Quigley, M. A. Goodrich, S. Griffiths, A. Eldredge, and R. W. Beard, "Target acquisition, localization, and surveillance using a fixed-wing mini-UAV and gimbaled camera," in *Proc. IEEE Int. Conf. Robot. Autom.*, Apr. 2005, pp. 2600–2605.

[25] M. Islam, M. Okasha, and M. M. Idres, "Trajectory tracking in quadrotor platform by using pd controller and LQR control approach," *IOP Conf. Ser. Mater. Sci. Eng.*, vol. 260, no. 1, 2017, Art. no. 012026.

[26] E. Fresk and G. Nikolakopoulos, "Full quaternion based attitude control for a quadrotor," in *Proc. Eur. Control Conf. (ECC)*, Jul. 2013, pp. 3864–3869.

[27] M. Rabah, A. Rohan, Y.-J. Han, and S.-H. Kim, "Design of fuzzy-PID controller for quadcopter trajectory-tracking," *Int. J. Fuzzy Logic Intell. Syst.*, vol. 18, no. 3, pp. 204–213, 2018.

[28] A. C. Woods and H. M. La, "Dynamic target tracking and obstacle avoidance using a drone," in *Proc. 11th Int. Symp. Vis. Comput.*, Las Vegas, NV, USA, Dec. 2015.

[29] C. Tingbin and Z. Qisong, "Robot motion planning based on improved artificial potential field," in *Proc. 3rd Int. Conf. Comput. Sci. Netw. Technol.*, Oct. 2013, pp. 1208–1211.

[30] ArduPilot Documentation Team. (2020). *ArduPilot*. Accessed: Jul. 3, 2020. [Online]. Available: https://ardupilot.org/ardupilot/

[31] PX4 Development Team. (2020). *PX4 Autopilot User Guide*. Accessed: Jul. 2, 2020. [Online]. Available: https://docs.px4.io/master/en/index.html

[32] A. Koubaa, Ed., *Robot Operating System (ROS)—The Complete Reference (Volume 1)* (Studies in Computational Intelligence Series), vol. 625, 1st ed. Cham, Switzerland: Springer, 2016.

HERATH MPC JAYAWEERA (Member, IEEE) received the B.Sc. special degree in physics from the University of Kelaniya, Sri Lanka, in 2011, and the M.Sc. degree in SEES from Middle East Technical University, Northern Cyprus Campus, in 2017. He is currently pursuing the Ph.D. degree with the Institute for Intelligent Systems Research and Innovation (IISRI), Deakin University, Australia. His research interests include UAV path planning, autonomous robotics, and artificial intelligent.

SAMER HANOUN received the Ph.D. degree from Deakin University, in 2009. He is currently an Associate Professor with the Institute for Intelligent Systems Research and Innovation (IISRI), Deakin University. His research interests include decision-making, many objective optimization, autonomous robotics, automation techniques for performance evaluation in simulation-based training, and knowledge-centric after action review frameworks.